

## SPERIMENTAZIONE SU PANNELLI MURARI CON APERTURE RINFORZATI CON FRP

### RESEARCH ON FRP STRENGTHENING OF URM WALLS WITH OPENING

**Tong Li**

**Nestore Galati**

**Antonio Nanni**

<sup>(1)</sup> University of Missouri-Rolla, 1870 Miner Circle, 65401 Rolla, MO - USA

#### SOMMARIO

Questo articolo presenta un'indagine sperimentale avente lo scopo di investigare l'efficacia nell'utilizzo sull'uso di barre in materiale composito a matrice polimerica (FRP) come rinforzo superficiale (near-surface mounted, NSM), e nella loro analisi numerica con un software agli elementi finiti. Sei provini, con diversi schemi di rinforzo, sono stati testati ciclicamente a taglio a diversi valori di sforzo assiale. Le differenti condizioni di rinforzo considerano l'uso di barre di vetro montate vicino la superficie, e disposte orizzontalmente, verticalmente o con una combinazione delle due. I risultati sperimentali hanno mostrato che l'incremento del carico assiale ha come conseguenza un aumento dei carichi ed una diminuzione degli spostamenti ultimi. L'efficacia delle barre composite in vetro è stata dimostrata grazie ad un miglioramento delle prestazioni dei pannelli murari rinforzati. Infine, il modello agli elementi finiti si è dimostrato efficace nel predire i risultati sperimentali con accettabile accuratezza.

#### ABSTRACT

The paper presents an experimental study aimed at investigating the efficiency of utilizing near-surface mounted (NSM) Glass Fiber Reinforced Polymer (GFRP) bars to strengthen unreinforced masonry (URM) walls and analyze it numerically with commercial finite element software. A series of 6 concrete masonry walls, unreinforced and/or strengthened with different strengthening schemes by GFRP bars, were subjected to a cyclic lateral force applied at the top of the walls and constant axial forces. The different reinforcement configurations include installing horizontal and/or vertical NSM FRP bars. Experimental results pointed out that though increase of vertical load may improve the lateral load-carrying capacity of the wall, it tends to decrease the ultimate displacement capacity. The experimental results demonstrated the effectiveness of FRP strengthening on improving the structural performance of URM walls. Numerical modeling predicted the test results with acceptable accuracy.

## **INTRODUCTION**

Masonry buildings constitute a large portion of the building stock throughout the world and failure of un-reinforced masonry (URM) walls is identified as one of the major causes of material damage and loss of human life during an earthquake. Moreover, walls are usually built with openings for doors and/or windows which weaken the ability of the walls to resist lateral forces. This led to an urgent need in developing effective and affordable retrofitting techniques to upgrade in-plane strength of masonry walls to resist earthquake loads.

In the last decade, FRP composites have been widely used for strengthening and retrofitting of concrete and masonry structures. Experimental tests showed the effectiveness of FRP strengthening in upgrading the structural behavior of URM walls ([1] and [2]). The FRP structural repointing technique was demonstrated being very effective on improving the structural performance of URM walls experimentally ([3]). The macro- and micro-modeling approaches have been adopted by researchers to investigate the behavior of masonry structure. The macro-modeling approach neglects the distinction between brick units and mortar joints by utilizing homogenization techniques ([4] and [5]) Alternately, the micro-modelling approach is a computationally expensive approach in which the masonry structure is modeled as a discontinuous assembly of blocks connected by discrete joints that are simulated by appropriate constitutive interface elements ([6] and [7]). Also discrete element methods were implemented analyzing masonry structures ([8] and [9]).

The present paper is devoted to the analysis of Glass FRP (GFRP) bars strengthened URM walls with openings. The GFRP bars were near-surface mounted (NSM) to both faces of the walls using a technique terms structural repointing, which is accomplished by embedding FRP bars with suitable paste in pre-cut grooves along the mortar joints. The GFRP laminates were bonded by manual lay-up on the wall surface. GFRP material was selected due to its high-strength, low modulus of elasticity (compatible with masonry) and low cost. Engineering simulation software, ANSYS, is adopted to model the behavior of masonry walls subjected to lateral in-plane loads. The effectiveness of the proposed model is evaluated by good agreement between experimental and theoretical values.

## **EXPERIMENTAL PROGRAM**

Six full scale rectangular concrete masonry walls, which were labeled as Walls 1A, 1B, 2A, 2B, 2C and 2D (Table 1), were tested. And each of the walls contained a rectangular opening which occupies 16% of the gross wall area. Two concentrated constant compressive forces were applied on the top of the walls at the middle of the piers as shown in Figure 1. A total compressive axial force of 32.4 kips (144.12 KN) was applied to walls 1A and 1B while a total compressive axial force of 24.5 kips (108.98 KN) was applied to walls 2A to 2D. Consequently, the average net area compressive stresses on the walls were 122.4 psi (0.84 MPa) and 89.3 psi (0.62 MPa), respectively. The horizontal force was applied in the middle of the top steel beam. Walls 1A and 1B were subjected to a cyclic load history while walls 2A to 2D were subjected to a fully reversed cyclic load history (Figure 2) with increased amplitude. The purpose of the load cycles was to simulate the behavior of masonry walls under earthquake load. In order to prevent tilting or twisting of the strengthened walls, the FRP reinforcement was installed symmetrically on both faces of each wall. The spacing between the horizontal GFRP bars was the nominal height of the masonry units and the vertical spacing between the vertical GFRP bars/laminates was half

of the nominal length of the units. Specimens were considered “failed” after reaching a pear load or when they became unstable.

**Table 1 Test Matrix**

Test Unit	Test Method	Retrofit Scheme
1A	Cyclic Racking Test	Control Unit –No Retrofit
1B	Cyclic Racking Test	8 0.25in. (6.35mm) Dia. Horizontal GFRP Bars
2A	Fully Reversed Cyclic Racking Test	Control Unit –No Retrofit
2B	Fully Reversed Cyclic Racking Test	8 0.25in. (6.35mm) Dia. Horizontal GFRP Bars
2C	Fully Reversed Cyclic Racking Test	8 0.25in. (6.35mm) Dia. Vertical GFRP Bars
2D	Fully Reversed Cyclic Racking Test	8 0.25in. (6.35mm) Dia. Horizontal GFRP Bars plus 8 - 2in. (50.8mm) wide Vertical GFRP Laminates

1A,2A      1B,2B      2C      2D

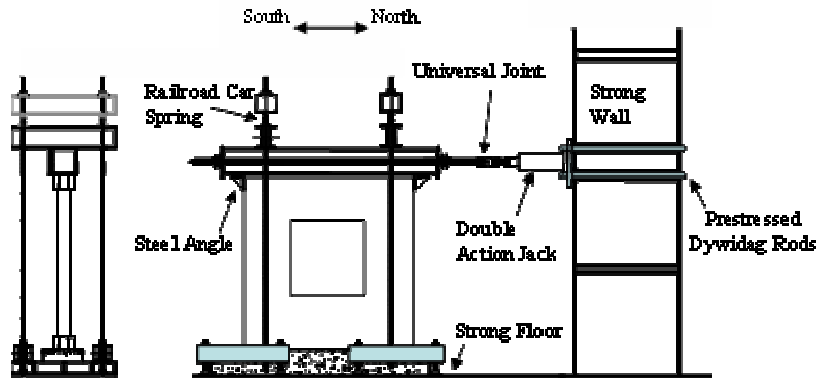


**Figure 1. Test Setup**

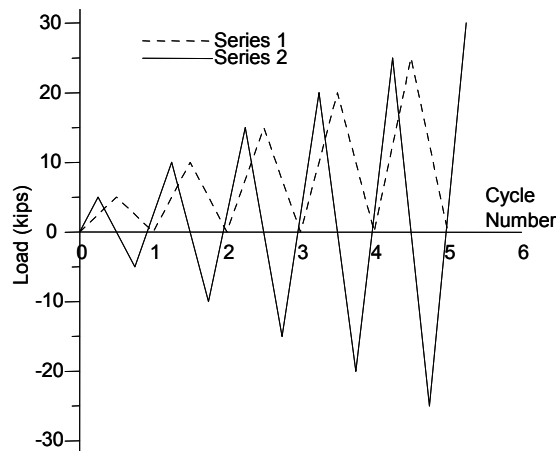


**Figure 2. Load Cycles**

The walls were constructed following a running bond pattern and had overall dimensions of the walls were 80x80x6 in. (2032x2032x152 mm). The dimension of the central opening was 32x32 in. (812.8 x812.8 mm). The masonry units, with nominal dimensions of 6x8x16 in. (152x203x406 mm), had a gross area of 84.89 in<sup>2</sup> (54700 mm<sup>2</sup>) and a net area of 54.89 in<sup>2</sup> (35400 mm<sup>2</sup>). A net area compressive strength of 2440 psi (16.8 MPa) was obtained with 3-block high masonry prisms (ASTM E477-84). The average thickness of the mortar joints was 0.375in. (9.5mm). A Type N mortar (ASTM C270) was used to build the walls, which has an average compressive strength of 1,570 psi (10.8 MPa) according to ASTM C109. The cross section of GFRP bars used in the program was 0.051 in<sup>2</sup> (33.2 mm<sup>2</sup>) with a tensile strength of 119.6 ksi (824 MPa) and a tensile elastic modulus of 7,276 ksi (50.2 MPa) ([10]). The cross section of one 4 in. (101.6 mm) wide GFRP laminates used in the program was 0.028 in<sup>2</sup> (17.8 mm<sup>2</sup>) with a gross-area tensile strength of 244.7 ksi (1687 MPa) and a tensile elastic modulus of 12,057 ksi (83.1 MPa) ([11]). The embedding material used for GFRP bars was an epoxy-based paste which has average 28-day strength of 2.68 ksi (18.5 MPa) ([10]).

Figure 1 shows a schematic of the test setup, which was similar to a typical Racking Test setup (ASTM 72). The horizontal load was applied in the south-north direction by a double-action hydraulic actuator that was fixed to the strong wall with pre-stressed high-strength steel bars. A universal joint was installed between the hydraulic actuator and the top steel beam to accommodate small distortions that might occur during the test. The wall was constructed directly on a concrete footing which was fixed to the strong floor. Two steel square beams, which were placed at the middle of the piers, were pressed to the top steel beam by two pairs of rail road springs to apply constant compression force and avoid rocking. The compression force was transferred to the bottom anchor steel beams. At each of wall corners, steel angles were installed to prevent the wall from sliding. To avoid local compression failure of the toe, a piece of plywood was placed between a steel angle and the masonry block. The load imposed on the wall was measured by load cells at the ends of the top steel beam. The in-plane displacement of the walls was measured by a displacement transducer mounted horizontally between the top course of the wall and an external reference frame. The shear deformation of the wall was measured by four Linear Variable Differential Transducers (LVDTs) diagonally mounted on both sides of each specimen. Strain gauges were attached to FRP reinforcement to monitor the strain. Instrumentation was connected to a data acquisition system acquiring data at 1 Hz.

## **EXPERIMENTAL RESULTS**

Though all specimens failed due to a combination of shear and rocking, the specimens exhibited different behavior with respect to different strengthening schemes. Figure 3 shows the cracks of specimens 2A to 2D. Two horizontal tensile cracks, developed at the bottom and top of the walls at the outset of the test, are not to be considered as essential as generally they are seldom observed in actual bearing walls. Diagonal tensile cracks in an inclined stair-step pattern along the head and bed joints, arising from two corners of the opening, were observed without significant increase in the applied load. Under increased loading conditions, newly developed rocking cracks which extend along the bed joints at the top or bottom of the weak piers that were produced by the central opening arose from the outside edges of the wall. These rocking and diagonal cracks divided the wall into four rigid parts that were forced to rotate against each other and resulted in considerable compressive stress concentration at the compression toes of the piers and the wall. The

local crushing at these locations could cause failure of the wall. And the abrupt increase of the displacement due to rocking of the piers could significantly reduce the stiffness of the wall.

At the ultimate stage, the pier that was under higher axial compressive force experienced a sudden and unstable failure when diagonal cracking propagate through it as a result of the increase of lateral deflection rather than of the lateral force. The four parts rotated against each other and the compression zone near the bottom of the piers decreased significantly even though there was trivial increase in lateral force. Finally, a collapse mechanism could form with either crushing of the compression toes, which changed the behavior of the wall to be similar to four rigid bodies connected by the hinges at the compression toes, or a complete diagonal crack going through the pier that was subjected to a higher axial compression force.

On the other hand, the spandrels governed the failure mode of the wall when the wall was reinforced with vertical FRP bars in the piers as the bars actually formed a strong column-weak beam system. Concentration of diagonal shear cracks was observed in the spandrels. Specimen 2C reached its ultimate state when the spandrel above the opening fractured thoroughly and the test was stopped when a diagonal tensile crack formed in the pier (Figure 3c). As shown in Figure 3d, specimen 2D reached its ultimate state when the compression toes of the wall crushed. A better ductility behavior of specimen 2D was exhibited than specimen 2C because the horizontal reinforcement in the spandrel held the fractured blocks together. It should also be noted that failure of GFRP bars was not observed in the experimental program. The strain recorded in the tests for horizontal and vertical GFRP bars indicated that on average the FRP bars developed 55% of their ultimate stress.

The load-displacement envelopes are shown in Figure 4. It is clear that the increase of applied vertical load on the wall only led to an increase in the initial stiffness of the wall and did not improve the in-plane load-carrying capacity of the wall due to the weak piers. Vertical reinforcement increased not only the lateral load-carrying capacity but also the stiffness as it was capable of restraining rocking of the piers. Strengthening with a combination of horizontal reinforcement in the spandrels and vertical reinforcement in the piers is the most efficient way to upgrade the structural behavior considering the improvement in the load-carrying capacity and the ultimate displacement capacity.

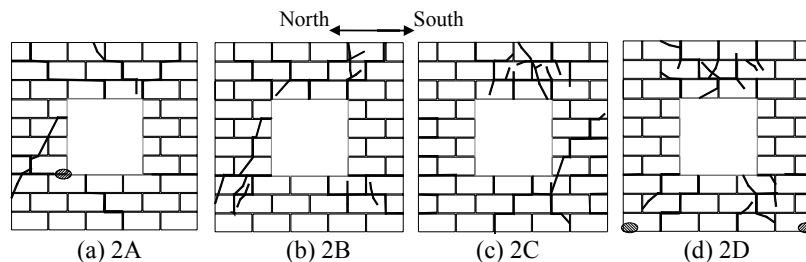


**Figure 3. Crack Pattern at Ultimate (2A-2D)**

## FORMULATION OF THE MODELING

In the FEM model, the brick units are depicted as an assemblage of plane stress 4-nodes elements, Plane 42, interacting with each other by the mortar joints which are modeled by zero thickness contact elements (Figure 5). A multi-linear isotropic hardening material is

adopted to model the behavior of masonry bricks (Figure 6). As limited by the program, no segment can have a slope less than zero the experimental compressive strength of masonry, which is taken from three-block-high stack-bonded prism tests, equals to 2440 psi (16.8 MPa).

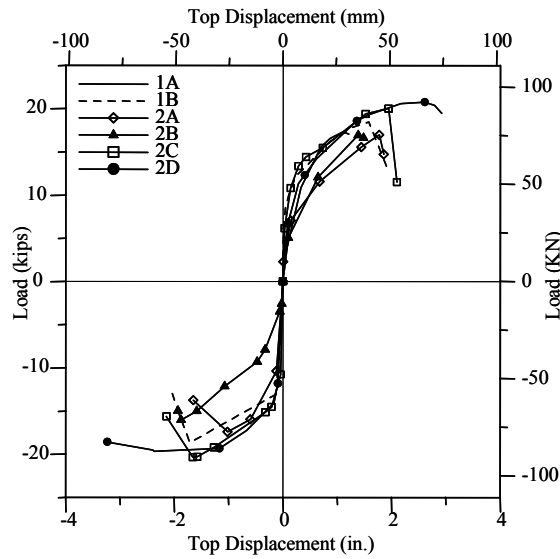


Figure 4. Load-Horizontal Displacement Envelopes

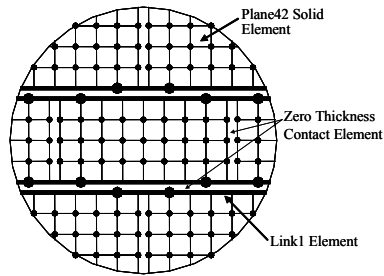


Figure 5. Finite Element Modeling

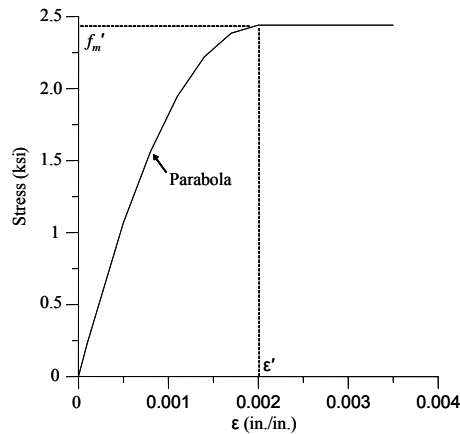


Figure 6. Material Model for Bricks

In the present analysis, essential nonlinear behavior in the panel is assumed to concentrate in the interfaces which were modeled with zero-thickness contact elements. For contact to occur, a stiffness relationship between two bodies must be established to avoid bodies passing through one another. The relationship is generated through an “elastic spring” that is placed between the two bodies, where the normal contact force is equal to the product of the contact stiffness ( $k_n$ ) and the penetration ( $\delta$ ). The value of  $k_n$  depends on the relative stiffness of the bodies in contact and can be specified by either a scaling factor or an absolute value. In the present analysis, the contact stiffness is a combined function of the interaction between the bricks and mortar joints, as well as the behavior of the mortar joints. The tangent penalty stiffness of the contact surface is calculated from the Poisson’s Ratio of mortar and the normal stiffness of contact surface.

Though there are a few other contact models available in ANSYS, a no separation contact model fits the requirements of current analysis best. The contact model not only permits sliding, but allows opening of the contact by adjusting the opening stiffness of the contact with a "weak-spring". This contact behavior is just what is wanted in the present analysis where separation is expected but a connection must be maintained to prevent rigid body motion. The normal and tangential contact stiffness were updated each sub-step based on the contact pair in the analysis. In the present analysis, different values were used for bed and head joints due to their dissimilar behavior. For bed joints, it was initially set to be equal to the normal contact stiffness. For the head joints, it was set to be a constant smaller value. The reason of this difference in the opening stiffness is that head joints are often not properly filled with mortar and shrinkage of the mortar, especially under poor curing conditions, may affect the bond strength between mortar and brick. The default value 0.1 is adopted for the penetration tolerance, which specifies an allowable maximum penetration of the contact.

The nonlinear behavior of joints is characterized by slip and separation taking place at the joint plane. The Coulomb friction model defines an equivalent shear stress  $\tau$ , at which sliding on the surface begins as a fraction of the contact pressure  $\sigma_n$  (Figure 7),

$$\tau = \tau_0 + \mu\sigma_n \quad (1)$$

where  $\mu$  is the friction coefficient and  $\tau_0$  specifies the cohesion sliding resistance which provides sliding resistance, even with zero normal pressure. Once the shear stress is exceeded, the two surfaces will slide relative to each other. Morbin ([11]) ran tests with three confinement stress and obtained  $\tau_0 = 58.01$  psi (0.4 MPa) and  $\mu = 0.668$  for the same type of masonry units and mortar. ANSYS also defines a maximum equivalent shear stress so that, regardless of the magnitude of the contact pressure, sliding will occur if the magnitude of the equivalent shear stress reaches this value (Figure 7). A reasonable upper estimate for this is the von Mises yield stress of the material adjacent to the surface.

A Link1 element of ANSYS was used to model the FRP bars in the analysis. This two-dimensional spar element is a uniaxial tension-compression element with two degrees of freedom at each node and no bending of the element is considered. The FRP bars were simulated as a series of continuous Link1 elements. Nodes of the FRP bars link elements were connected to those of adjacent brick solid elements in order to satisfy the perfect bond assumption (Figure 5).

The analysis can take into account basic types of failure modes affecting both the mortar joints and the units. In general, tensile and shear damage is assumed to concentrate in the relatively weak joints as proven to be true for most masonry shear wall panels. The augmented Lagrangian method is used for the surface-to-surface contact elements. Approximate stress and strain material failure criteria provided by ANSYS were adopted to identify the ultimate stage of the analysis.

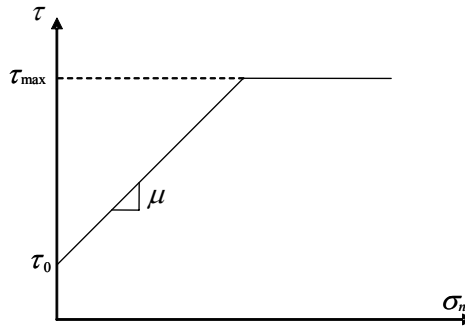


Figure 7. Friction Model

## NUMERICAL EXAMPLES

The proposed ANSYS model was applied to some numerical examples in order to test the numerical procedure. An example simulating compressive test of masonry prism is presented first in order to validate the proposed model, understand and determine the parameters defining the contact elements and compare the numerical results with the experimental data. The compressive test is conducted on prisms as tested in the experimental program. The results calculated using different value of contact stiffness are compared with the experimental results (Figure 8). The penalty contact stiffness is expressed as a factor of the elasticity of the mortar. From the results it can be concluded that when the contact stiffness factor equal to 0.11, it best simulates the test results. This value is adopted for further analysis. Material properties acquired from experimental tests are illustrated in Table 2. The primary parameters used in the modal analysis for contact elements are summarized in Table 3.

The proposed model is used to simulate experimental tests on masonry walls with openings. The bottom concrete beam was modelled as a rigid surface. The top steel beam was modelled as an assemblage of plane stress 4-nodes elements. To simulate the boundary conditions provided by the steel angles at the top of the wall, the top of the wall was coupled with the bottom of the steel beam to have the same displacement in the x direction. The model analysis was run in two steps: first the vertical compression load was applied to the upper face of the beam at two locations, then the monotonically increasing horizontal load was applied at the centroid of the end section of the top beam.

In the present analysis, the final failure mode of the specimen is identified by a combination of maximum tensile strength and compressive stresses where the location of the diagonal tensile crack was given by the diagonal compression strut and the maximum tensile stress at the strut. The failure modes of specimens 1B, 2A and 2B are similar to that of specimen 1A. Failure mode of specimen 2C is diagonal cracking of the weak piers. Specimen 2D reached its ultimate capacity when the compression toes crushed. Diagonal tensile crack could not be developed due to the reinforcement. The numerical model captures well the experimental behavior, as demonstrated in Table 4.

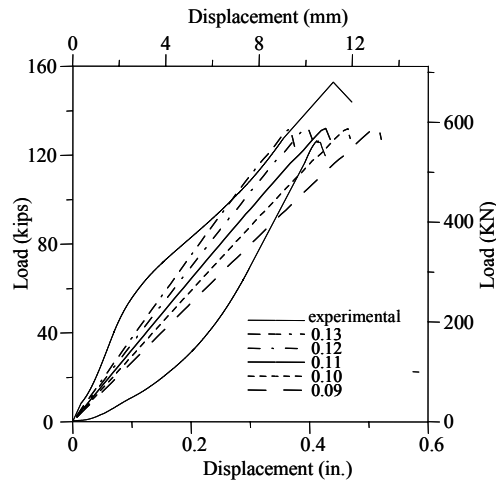


**Figure 8. Results of Compressive Prisms**

**Table 2. Summary of Material Properties**

Material	Elastic Modulus ksi (MPa)	Compressive Strength psi (MPa)	Possion Ratio	Tensile Strength ksi (MPa)	Cross Sectional Area in <sup>2</sup> (mm <sup>2</sup> )
Brick	2,296 (15,830)	2,440 (16.9)	0.2	0.244 (1.69)	54.89 (35,400)
Mortar	114.616 (790)	1,570 (10,825)	0.05	0.114 (0.786)	N.A.
GFRP Bar	7,276 (50.2)	N.A.	N.A.	119.6 (824.6)	0.051 (33.2)

**Table 3. Summary of Contact Parameters**

Material	Bed Joint	Head Joint
contact stiffness FKN: psi (MPa)	12,608 (86.93)	12,608 (86.93)
tangent contact stiffness FKT: psi (MPa)	6004 (41.40)	6004 (41.40)
opening contact stiffness KFOP: psi (MPa)	12,61 (86.93)	1.261 (0.00869)
penetration tolerance: in. (mm)	0.2 (5.08)	0.2 (5.08)
Max. initial friction coefficient MU	0.668	0.668
Contact cohesion COHE: psi (MPa)	58 (0.4)	58 (0.40)
Max. friction stress TAUMAX: psi (MPa)	453 (3.12)	453 (3.12)
Average contact surface length: in. (mm)	2.0 (50.8)	2.0 (50.8)
Average contact pair depth: in. (mm)	2.0 (50.8)	2.0 (50.8)
pinball region: in. (mm)	4 (101.6)	4 (101.6)
initial contact closure: in. (mm)	0.4 (10.16)	0.4 (10.16)

In general, the main conclusion of the verification examples is that the finite element model can be used to simulate the behavior of the specimens, i.e., the cracking pattern, the failure mode, the ultimate load, conversely the determination of ultimate load is difficult.

## SUMMARY AND CONCLUSIONS

It can be concluded from the experimental program that FRP composites are efficient in improving the performance of URM walls. Vertical reinforcement in the piers significantly increased the stiffness, maximum lateral load-carrying capacity and energy dissipation capacity of URM walls. However, it impaired the maximum displacement capacity.

Strengthening with a combination of horizontal reinforcement in the spandrels and vertical reinforcement in the piers significantly improved the overall structural behavior of the walls including lateral load-carrying capacity, stiffness, energy dissipation capacity and maximum displacement capacity.

**Table 4. Ultimate State**

Test Unit	Experimental		FEM	
	Load kips (KN)	Displacement in. (mm)	Load kips (KN)	Displacement in. (mm)
1A	17.3 (77.0)	1.20 (30.5)	17.7 (78.7)	1.10 (27.9)
1B	18.5 (82.3)	1.58 (40.2)	17.7 (78.7)	1.16 (29.5)
2A	17.0 (75.5) -17.4 (-77.4)	1.78 (45.1) -1.02 (-25.9)	17.7 (78.7)	1.29 (32.8)
2B	16.9 (75.3) -16.0 (-71.2)	1.40 (35.5) -1.89 (-48.1)	18.1 (80.5)	1.08 (27.4)
2C	20.0 (89.0) -20.3 (-90.3)	1.94 (49.3) -1.66 (-42.2)	20.6 (91.6)	1.99 (50.5)
2D	20.6 (91.6) -19.6 (-87.2)	2.18 (55.3) -2.37 (-67.0)	22.9 (101.9)	2.40 (61.0)

The proposed model is capable of capturing some basic mechanisms that characterize the behavior of the masonry walls, namely, tensile cracking failure of the mortar joints, shear sliding of the mortar joints as well as fracturing of the masonry units due to high friction in joints at high values of normal stress which lead to high tensile stress in the units. A model of this nature may also be used as a research tool for calibrating the properties of the masonry components can be varied individually. The accuracy of the analysis is influenced by the degree of variability inherent in the material properties.

## ACKNOWLEDGEMENTS

The authors would like to acknowledge the support of the National Science Foundation Industry/University Cooperative Research Center at the University of Missouri-Rolla. Financial support was also provided under NSF Grant Award NSF CMS-0201815.

## REFERENCES

- [1] Laursen P. T., Seible F., Hegemier G. A., Innamorato D. (1995). "Seismic retrofit and repair of masonry walls with carbon overlays." Non-metallic (FRP) reinforcement for concrete structures, L. Taerwe, ed., 616-623.
- [2] Ehsani, M R. Saadatmanesh, H. Al-Saidy, A. (1997). "Shear Behavior of URM Retrofitted with FRP Overlays." Journal of Composites for Construction, 1(1), 17-25.
- [3] Tumialan, J.G., Huang P-C., Nanni, A., and Silva, P. (2001). "Strengthening of Masonry Walls by FRP Structural Repointing." Non-metallic reinforcement for Concrete Structures - FRPRCS-5, Cambridge, England, July 16th-18th, 1033-1042.
- [4] Dhanasekar, M., Kleeman, P. W., and Page, A. W. (1985). "Biaxial stress-strain relations for brick masonry." J. Struc. Engrg., ASCE, 111(5), 1085-1100.
- [5] Middleton, J., Pande, G. N., Liang, J. X., and Kralj, B. (1991). "Some recent advances in computer methods in structural masonry." Computer methods in structural masonry, J.

- Middleton and G. N. Pande, eds., Books and Journals International, Swansea, U.K., 1-21.
- [6] Rots, J G. (1991). "Numerical simulation of cracking in structural masonry." *Heron*, 36(2), 49-63.
- [7] Gambarotta Luigi and Lagomarsino Sergio. (1996). "Finite element damage model for the evaluation and rehabilitation of brick masonry shear walls." *Worldwide Advances in Structural Concrete and Masonry Structures Congress – Proceedings*, ASCE, New York, NY, USA., April 15-18, 72-81.
- [8] Camborde F., Mariotti C. and Donze F.V. (2000). "Numerical study of rock and concrete behaviour by discrete element modelling." *Computers and Geotechnics*, 27, 225–247.
- [9] Formica G., Sansalone V., and Casciaro R.. (2002). "A mixed solution strategy for the nonlinear analysis of brick masonry walls." *Computer Methods in Applied Mechanics and Engineering*, 191(51-52), 5847-5876.
- [10] Grando Stefano. (2001). "Shear Strengthening of URM Walls with FRP Systems." Report CIES 01-48, Center for Infrastructure Engineering Studies, University of Missouri-Rolla, Rolla, MO, (<http://campus.umr.edu/rb2c/>).
- [11] Morbin A. and Nanni A. (2002). "Strengthening of Masonry Elements with FRP Composites." Report CIES 02-23, Center for Infrastructure Engineering Studies, University of Missouri-Rolla, Rolla, MO, (<http://campus.umr.edu/rb2c/>).